CO and NO Adsorption and Dissociation at the B-Mo_2C(0001) Surface: A Density Functional Theory Study

Xue-Rong Shi,[†,‡,§] Jianguo Wang,*[,‡] and Klaus Hermann*[,†]

Theory Department, Fritz-Haber-Institut der MPG, Faradayweg 4-6, D-14195 Berlin, Germany, State Key Laboratory of Coal Conversion, Institute of Coal Chemistry, Chinese Academy of Sciences, Taiyuan, Shanxi 030001, People's Republic of China, and Graduate University of the Chinese Academy of Sciences, Beijing 100039, People's Republic of China

Received: December 21, 2009; Revised Manuscript Received: June 25, 2010

Adsorption and dissociation of CO and NO molecules at the Mo- and C-terminated β-Mo_2C(0001) surfaces has been investigated systematically using density functional theory methods together with cluster models. The calculations yield stable CO and NO adsorption for both surface terminations, suggesting strong adsorbate binding. Molecular adsorption of CO exhibits similar stability for the two terminations, while the molecular NO adsorbate prefers Mo termination over C termination. Computed vibrational frequencies of CO and NO are compared with data from infrared (IR) spectroscopy, allowing a detailed interpretation and assignment of the different features in the experimental spectra. C, N, and O atoms are quite strongly bound at the β-Mo_2C surface, where at the Mo-terminated surface, hollow sites are energetically preferred. For the C termination, only oxygen adsorbs near carbon sites, whereas C and N stabilize above Mo substrate atoms or in hollow sites. Dissociative adsorption of NO is energetically preferred over molecular adsorption, while for CO, the two types are energetically similar. Dissociation barriers of adsorbed NO are lower than those for CO, which is consistent with the experimental results. The barrier calculations show also that dissociation prefers the Mo-terminated over the C-terminated surface.

1. Introduction

Transition-metal carbides have attracted great interest because of their exciting physical and chemical properties, for example, their extreme hardness,[1] high melting points,[2] and high electrical as well as thermal conductivity.[3] In addition, β-molybdenum carbide (β-Mo_2C)-based catalysts exhibit excellent catalytic activity in a wide variety of reactions, such as the hydrogenation of benzene,[4,5] the hydrogenolysis of alkanes,[6] and the isomerization of alkanes.[7] Here, infrared (IR) spectroscopy using small probe molecules provides a convenient way to characterize active surface sites of the catalysts where CO and NO are found particularly suitable. The adsorption of these molecules at supported Mo-based catalysts has been well studied experimentally.[8–17] Wu et al. investigated CO adsorption on a fresh Mo_2C/Al_2O_3 catalyst by using in situ Fourier transform infrared (FT-IR) spectroscopy, where an absorption band at 2054 cm^{-1} was attributed to CO adsorbed at Mo^{x+} ($0 < x < 2$) sites, forming linear MoCO groups.[18] Further, a band at 2196 cm^{-1} was assigned to a CCO species that was created by the reaction of CO with surface carbon atoms at 1033 K. Aegerter et al. observed a broad band at 2178 cm^{-1} with a weak shoulder at 2060 cm^{-1} in IR spectra of CO on Mo_2C/Al_2O_3 at 130 K, where the band at higher wavenumbers was assigned to CO adsorbed at Mo^{4+} and the shoulder to CO adsorbed at Mo^{2+}.[8] Using reflectance absorbance infrared spectroscopy (RAIRS) and thermal desorption (TDS) measurements, Wang et al. studied CO adsorption on a clean β-Mo_2C film, where adsorption at 100 K was characterized by a single CO vibrational stretching frequency, typical of on-top adsorption, which increased from 2057 to 2072 cm^{-1} as a function of increasing coverage.[16] They also observed that the vibrational spectrum for adsorbed NO at 100 K yields a band at 1780 cm^{-1} with a coverage-dependent position shifting from 1780 cm^{-1}at low coverage to 1820 cm^{-1} at saturation coverage for a temperature of 100 K. The authors attributed this peak to a terminally bound NO species at the surface. Complementary thermal desorption results showed that almost all adsorbed NO dissociates, whereas only up to 10% of adsorbed CO undergoes decomposition. Siaj et al. studied dissociative adsorption of NO at β-Mo_2C by RAIRS and observed a band at 989 cm^{-1} with a shoulder at 942 cm^{-1}, which they assigned to Mo−O vibrational modes of the adsorbate rather than Mo−N modes.[17]

Considering the vast number of experimental investigations on the catalytic performance of molybdenum carbides, only rather limited theoretical research has been performed on a fundamental understanding of active sites of molybdenum carbide surfaces. Most theoretical studies focused on the bulk structure[19–21] and hydrotreating reactions,[22–24] while only a few considered the adsorption of CO and NO on β-Mo_2C surfaces. Bulk β-Mo_2C is described by a disordered hexagonal crystal lattice in which Mo atoms form a hexagonal close-packed array and C atoms occupy one-half of the octahedral interstitial sites in a random way.[19,20] From X-ray diffraction and ab initio calculations, Haines et al. proposed an eclipsed configuration for β-Mo_2C with Mo−C−Mo−C stacking, where C atoms occupy one-half of the octahedral interstitial sites in the second layer and the other half in the fourth layer.[25] In addition, Tominaga and Nagai considered a structure with a Mo−C−Mo−Mo−C stacking pattern where every fourth layer with C atoms was missing in theoretical studies on the water−gas shift, methane reforming, and thiophene hydrodesulfurizationon.[22–24]

* To whom correspondence should be addressed. E-mail: hermann@fhi-berlin.mpg.de (K.H.); iccjgw@sxicc.ac.cn (J.W.).
† Fritz-Haber-Institut der MPG.
‡ Institute of Coal Chemistry, Chinese Academy of Sciences.
§ Graduate University of the Chinese Academy of Sciences.

10.1021/jp912036z
Published on Web 07/22/2010

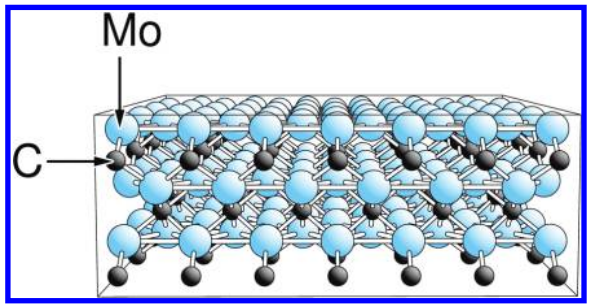

Figure 1. Crystal structure of β-Mo_2C with six atom layers along (0001); see text. Molybdenum (carbon) atoms are shown by large (small) shaded balls with connecting sticks to visualize atom coordination.

Further, C. Pistonesi et al.[26] have investigated methanol adsorption and dissociation at the β-Mo_2C(0001) surface, where the β-Mo_2C phase was reported as an orthorhombic crystal structure with experimental lattice constants $a = 5.195$ Å, $b = 6.022$ Å, and $c = 4.725$ Å.[27] This crystal structure was termed α-Mo_2C by other groups[28–36] and considered in theoretical studies using cluster as well as periodic models.[37–39]

In this work, we present results from theoretical studies on the adsorption and dissociation of CO and NO at the β-Mo_2C(0001) surface in order to obtain basic information about active surface sites of molybdenum carbide. Surface cluster models together with ab initio DFT methods are employed to examine geometrical features, relative stability of the adsorbates, as well as their vibrational properties, which are used to interpret corresponding IR spectra. In section 2, we describe computational details of the present work, while in section 3, we present results of the calculations. Finally, in section 4, we summarize our results and conclusions.

2. Models and Methods

In this study, the β-Mo_2C substrate is modeled by an eclipsed configuration with Mo−C−Mo−C stacking along the [0001] direction, where C atoms occupy one-half of the octahedral interstitial sites in the second and fourth layers each; see Figure 1. This bulk structure has been shown to be energetically more favorable[25] and seems to be more balanced than the geometry applied by Tominaga and Nagai.[22] The (0001) surface, well-accepted to be the active surface for catalytic reactions,[22–24,40] can be either molybdenum- or carbon-terminated; see Figure 1.

In this work, local surface regions of the substrate are simulated by large surface clusters, which were selected after careful testing according to size, shape, and electronic charge distribution, given by electron density maps and populations. Here, $Mo_{31}C_{12}$ surface clusters, shown in Figure 2a, b, were found to yield a good compromise between numerical accuracy and computational effort for both terminations. These clusters include four substrate layers, two molybdenum and carbon each, and their central surface region is affected very little by adding Mo and C atoms at the cluster periphery. Molecular CO and NO as well as atomic C, N, and O adsorption is examined by adding the corresponding species near high-symmetry surface sites of the substrate clusters (see Figure 2a, b) and optimizing their geometry to yield local equilibrium configurations (verified by subsequent vibrational analyses). The geometric optimizations include always all atoms of the adsorbate particles and their local substrate environment to account for surface relaxation in response to the presence of the adsorbates. Here, first and second nearest-neighbor substrate atoms are found to be

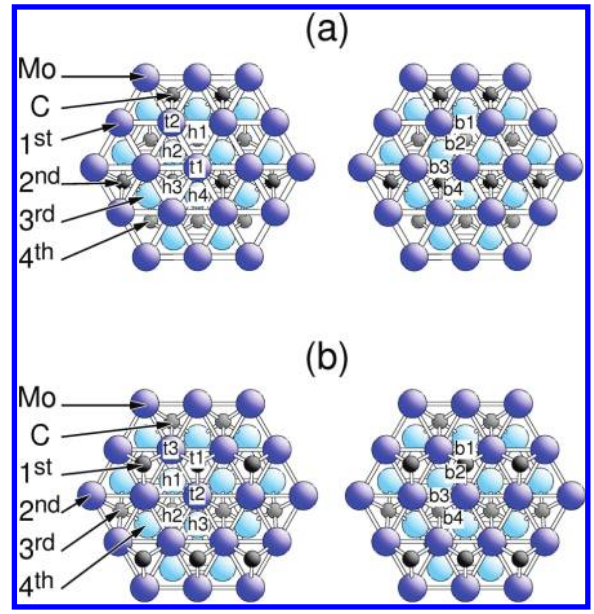

Figure 2. Top view of cluster models for (a) Mo termination and (b) C termination of the β-Mo_2C(0001) surface. Molybdenum (carbon) atoms are shown by large (small) balls with layer-dependent painting and connecting sticks visualizing atom coordination. The adsorption sites, top (t), bridge (b), and hollow (h), are indicated by corresponding labels.

sufficient to obtain reliable binding energies. This was tested by comparative calculations with varying relaxation environments.

Further, adsorption at the $Mo_{31}C_{12}$ substrate clusters is calculated for surface sites near the cluster center as well as at symmetry-equivalent sites near the cluster edge in order to examine the influence of edge effects on geometry and energetics. The comparison yields differences between corresponding adsorption energies E_{ads}, which can be ignored for the present purpose. As an example, we mention molecular CO adsorption where E_{ads} differences are always below 0.1 eV. This suggests that cluster edge effects contribute very little to adsorption and reaction near the surface centers of the present $Mo_{31}C_{12}$ clusters, thus making an additional cluster embedding unnecessary.

A simulation of the present system with its isolated adsorbate particles by periodic supercell calculations would have required rather large supercells, connected with sizable computational effort. However, the physical/chemical results are not expected to deviate from those of the present calculations applying well-chosen surface clusters.

Electronic ground states and derived properties of the clusters are calculated using density functional theory (DFT) together with generalized gradient-corrected exchange and correlation functionals according to Perdew, Burke, and Ernzerhof (RPBE).[30,41] The Kohn−Sham orbitals are represented by linear combinations of atomic orbitals (LCAO) using extended basis sets of contracted Gaussians. In the ground-state calculations and corresponding geometry optimizations, carbon, nitrogen, and oxygen are represented by all-electron DZVP basis sets ([9s5p1d] contracted to [3s2p1d] each), while molybdenum is described by a valence basis set ([8s7p5d] contracted to [6s5p4d]) for its 14 outermost electrons together with an effective core potential (ECP) to represent the atom core. Electronic ground states are evaluated for the appropriate spin multiplets by using spin polarization, that is, singlet CO, doublet NO, triplet C, O, and quartet N in gas phase, while the adsorbate clusters are determined as singlet or doublet states. All calculations are performed using the DFT cluster code StoBe.[42]

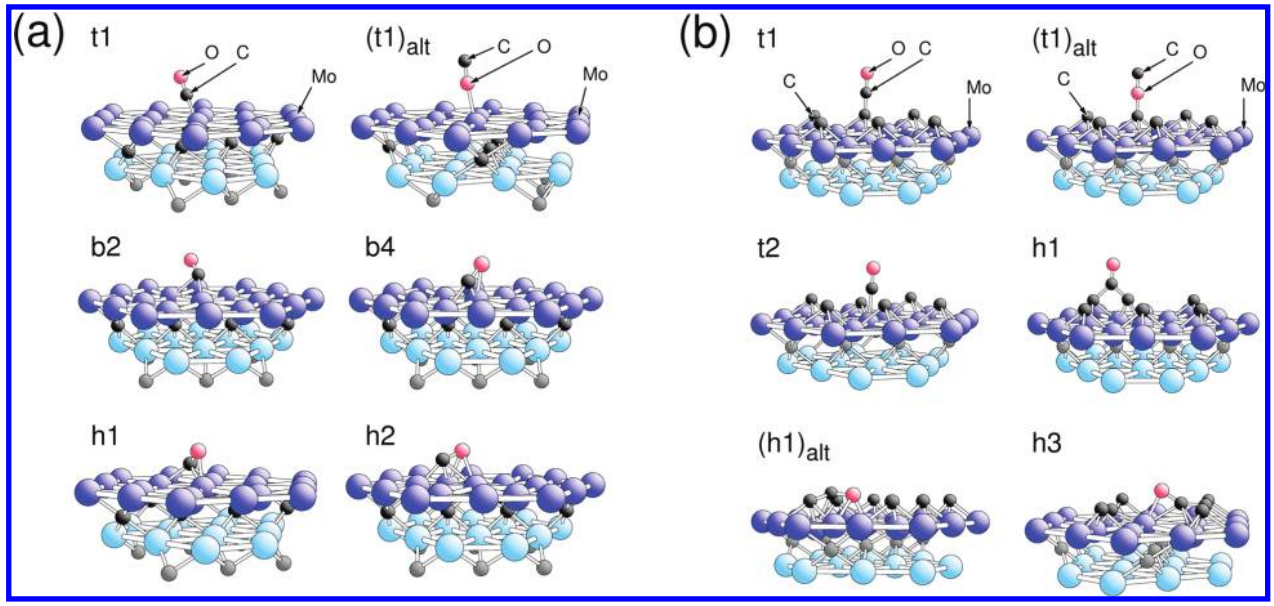

Figure 3. Equilibrium geometries of molecular CO adsorption at the β-$Mo_2C(0001)$ surface with (a) Mo termination and (b) C termination. Molybdenum (carbon, oxygen) atoms are shown by large (small) balls with different painting and connecting sticks visualizing atom coordination. The labels refer to adsorption sites as defined in Figure 2; see also text.

Adsorption energies E_{ads} are evaluated from differences of corresponding cluster total energies, for atomic/molecular adsorption defined by

$$E_{ads}(\mathrm{Ad}) = E_{tot}(\mathrm{SubAd}) - E_{tot}(\mathrm{Sub}) - E_{tot}(\mathrm{Ad}) \quad (1)$$

where Sub = $Mo_{31}C_{12}$ represents a substrate cluster of the β-$Mo_2C(0001)$ surface and Ad = C, N, O, CO, NO refers to the adsorbates. Negative E_{ads} values denote stable chemisorption, while positive values refer to metastable adsorption. In addition to molecular adsorption of CO and NO with energies defined by eq 1, we consider also dissociative adsorption, where adsorption energies E_{ads}' are given by

$$E_{ads}'(\mathrm{XO}) = E_{tot}(\mathrm{Sub{-}X{-}O}) - E_{tot}(\mathrm{Sub}) - E_{tot}(\mathrm{XO}) \quad (2)$$

with Sub = $Mo_{31}C_{12}$ representing a cluster of the clean β-$Mo_2C(0001)$ surface, Sub−X−O denoting the cluster with X, O atoms adsorbed simultaneously, and XO = CO, NO referring to the gas-phase molecules. Thus, the difference $\Delta E = E_{ads}(\mathrm{XO}) - E_{ads}'(\mathrm{XO})$ characterizes the binding between the two molecular components X, O at the surface.

CO as well as NO dissociation at the β-$Mo_2C(0001)$ surface is studied by considering the molecular species and its atomic components adsorbed at their equilibrium sites. Then, corresponding reaction paths, transition-state (TS) geometries, and energy barriers are calculated by applying the nudged elastic band (NEB) method.[43] Here, nine geometry images along the reaction path are considered for each NEB cycle. The TS configurations are verified by vibrational analyses where, in all cases, only one imaginary frequency is found.

Vibrational frequencies of the adsorbates, molecular and atomic, are evaluated by applying the harmonic approach to the corresponding surface clusters. For adsorbed molecular CO and NO, only intra-atomic vibrations are listed, while for atomic O and N adsorption (also resulting from dissociative NO adsorption), vibrations including nearest-substrate-neighbor atoms are given. For comparison with experiment, the calculated frequencies for the CO and NO adsorbates are scaled by factors of 1.026 and 1.015, respectively, which reflects the differences between measured and calculated frequencies of the corresponding gas-phase molecules.

3. Results and Discussion

Adsorption at the molybdenum-terminated (0001) surface of β-Mo_2C is examined for 10 different adsorption sites, as shown in Figure 2a, two top (t1 and t2), four bridge (b1, b2, b3, and b4), and four hollow sites (h1, h2, h3, and h4), while for the carbon-terminated surface, 10 analogous adsorption sites, three top (t1, t2 and t3), four bridge (b1, b2, b3, and b4), and three hollow sites (h1, h2, and h3) are considered; see Figure 2b.

3.1. Molecular CO Adsorption at β-$Mo_2C(0001)$. Of the 10 different adsorption sites at the Mo-terminated surface (see Figure 2a), only 5 sites, t1, b2, b4, h1, and h2, yield stable molecular adsorption, where equilibrium geometries are shown in Figure 3a. Calculated adsorption energies E_{ads} according to eq 1, selected equilibrium distances, and adsorbate charges (from Mulliken analyses) are given in Table 1a. Obviously, the three sites t1, b2, and h1 result in very similar adsorption energies, −1.91 to −1.99 eV, suggesting the strongest chemisorptive binding, while the h2 and b4 sites with E_{ads} = −1.60 and −1.11 eV, respectively, are energetically less favorable. Here, CO stabilizes at the t1 site in a tilted geometry, with its C end pointing toward the substrate. CO at the h1 (b2) site binds with an equal (slightly lower) adsorption energy and is also tilted; see Figure 3a. In contrast, CO approaching near the t2, b3, and h3 sites of the surface leads to adsorption at the b2 site, and CO near the b1 and h4 sites will adsorb at the h1 and t1 sites, respectively. Interestingly, the t1 site offers also an alternative adsorbate geometry where CO binds with its O end pointing toward the substrate. However, this geometry, labeled $(t1)_{alt}$ in Table 1a and Figure 3a, is much less stable, E_{ads} = −0.05 eV, than the initial t1 geometry. Table 1a lists also Mulliken charges of the CO adsorbate, which indicate that for all stable sites, there is electron transfer from the substrate to the adsorbate, yielding a negatively charged CO species.

Of the 10 different adsorption sites at the C-terminated surface (see Figure 2b), only 4 sites, t1, t2, h1, and h3, yield stable

TABLE 1: Molecular CO Adsorption at β-Mo_2C(0001) for (a) Mo Termination and (b) C Termination[a]

(a) Molybdenum Termination.

site		E_{ads}	$d_{C-O}/d_{C-Mo}/d_{O-Mo}$	Q_{CO}
top	t1	−1.99	1.21/1.99/−	−0.45
	$(t1)_{alt}$	−0.05	1.16/−/2.16	−0.13
	t2	→ b2	−	−
bridge	b1	→ h1	−	−
	b2	−1.91	1.23/1.98, 2.28/−	−0.54
	b3	→ b2		
	b4	−1.11	1.23/2.08, 2.30/2.35	−0.51
hollow	h1	−1.99	1.30/2.15, 2.08,2.16/2.05	−0.67
	h2	−1.60	1.27/2 × 2.28, 1.98/2.34, 2.30	−0.57
	h3	→ b2	−	−
	h4	→ t1	−	−
free CO		−	1.156/−, −/−	0.00

(b) Carbon Termination

site		E_{ads}	$d_{C-O}/d_{C-Mo}/d_{O-Mo}/d_{C-C}$	Q_{CO}
top	t1	−1.94	1.18/−/−/1.32	0.05
	$(t1)_{alt}$	2.17	1.19/−/1.39/−	−0.11
	t2	−1.02	1.16/2.04/−/−	−0.02
	t3	→ h1	−	−
bridge	b1	→ t1	−	−
	b2	→ t1	−	−
	b3	→ t2	−	−
	b4	→ t2	−	−
hollow	h1	−1.42	1.23/−/−/1.46,1.48	−0.02
	$(h1)_{alt}$	−0.78	1.40/2.25/2.21,2.23/1.46, 1.47	−0.23
	h2	→ t2	−	−
	h3	−1.53	1.28/2.40, 2 × 2.35/2.19/−	0.02

[a] The tables list CO adsorption energies E_{ads} (in eV), selected bond distances, d_{C-O}, d_{C-Mo}, and d_{O-Mo} (in Å), and Mulliken charges Q_{CO} of the CO adsorbate (in au). The adsorption sites are denoted as shown in Figure 2. Stable ($E_{ads} < 0$) or metastable ($E_{ads} > 0$) adsorption sites are included numerically, while unstable sites are denoted by arrows pointing to the nearest stable site; see text.

molecular adsorption, with equilibrium geometries shown in Figure 3b. Calculated adsorption energies E_{ads}, selected equilibrium distances, and adsorbate charges (from Mulliken analyses) are given in Table 1b. For this termination, the energetically most favorable site is t1, where CO adsorbs on top of a surface carbon to form a CCO species (see Figure 3b) with $E_{ads} = -1.94$ eV, similar in energy to the t1 site of the Mo-terminated surface. The next stable sites are hollow-type h3 (see Figure 3b) with $E_{ads} = -1.53$ eV, where CO lies almost flat at the surface, and hollow-type h1 (see Figure 3b) with $E_{ads} = -1.42$ eV, where CO adsorbs with its C end almost perpendicular to the surface between two carbon atoms of the substrate. The other stable but less favorable site is t2, where CO stabilizes on top of a Mo atom of the surface with $E_{ads} = -1.02$ eV. An alternative h1 site, labeled $(h1)_{alt}$ in Table 1b, where CO adsorbs almost flat at the surface, reflects weaker binding, with $E_{ads} = -0.78$ eV. CO near any of the bridge sites, b1−b4, of the surface leads to adsorption at the top sites t1 (starting from b1, b2) and t2 (starting from b3, b4). In addition, CO near the h2 and t3 sites will adsorb at the t2 and h1 sites, respectively. As for the Mo termination, the t1 site of the C termination allows an alternative adsorbate geometry where CO binds with its O end pointing toward the substrate and forming a COC species, labeled $(t1)_{alt}$ in Table 1b and Figure 3b, which is metastable with $E_{ads} = 2.17$ eV. The analysis of Mulliken charges of the CO adsorbate, included in Table 1b, shows that charge transfer from the substrate to the adsorbate is much less pronounced for the carbon than that for the molybdenum-terminated surface.

3.2. Molecular NO Adsorption at β-Mo_2C(0001). As for CO adsorption, 10 different adsorption sites at the Mo-terminated surface are examined (see Figure 2a), where 6 sites, t1, t2, b2, h1, h2, and h4, yield stable molecular adsorption with equilibrium geometries shown in Figure 4a. Calculated adsorption energies E_{ads} according to eq 1, selected equilibrium distances, and adsorbate net charges (from Mulliken analyses) are listed in Table 2a. Here, the hollow site h1, where the N end of NO sits in a hollow site and the O end sits on top of a Mo atom of the substrate surface (see Figure 4a), is energetically the most favorable, with $E_{ads} = -3.45$ eV. The other five sites, t1, t2, b2, h2, and h4, are energetically rather similar, with E_{ads} ranging between −2.70 and −2.99 eV. In contrast, NO approaching near the b1, b3, b4, and h3 sites of the surface leads to adsorption at the t1, b2, h4, and h2 sites, respectively. As for CO adsorption, the t1 site allows an alternative adsorbate geometry, labeled $(t1)_{alt}$ in Table 2a and Figure 4a, which is metastable, $E_{ads} = 0.11$ eV, and where NO binds with its O end pointing toward the substrate. While the intermolecular distance d_{N-O} of the NO adsorbate increases only slightly for the stable top and bridge sites, if compared with the gas-phase molecule, the increase for the hollow sites is much larger. This can be understood as due to adsorption-induced N−O bond weakening depending on the sites. The calculations yield for all sites an electron transfer from the substrate to the adsorbate, resulting in negatively charged NO species; see the Mulliken charges in Table 2a. Here, the actual negative charge is larger for the hollow site than that for the other sites. The transferred electrons occupy antibonding NO orbitals, thus weakening the interatomic N−O bond where the effect is larger for the hollow site than that for the other sites. Overall, adsorption energies of NO at the Mo-terminated (0001) surface of β-Mo_2C are found to be larger in absolute size compared with those of CO, suggesting chemisorptive bonds which are stronger for NO than those for CO.

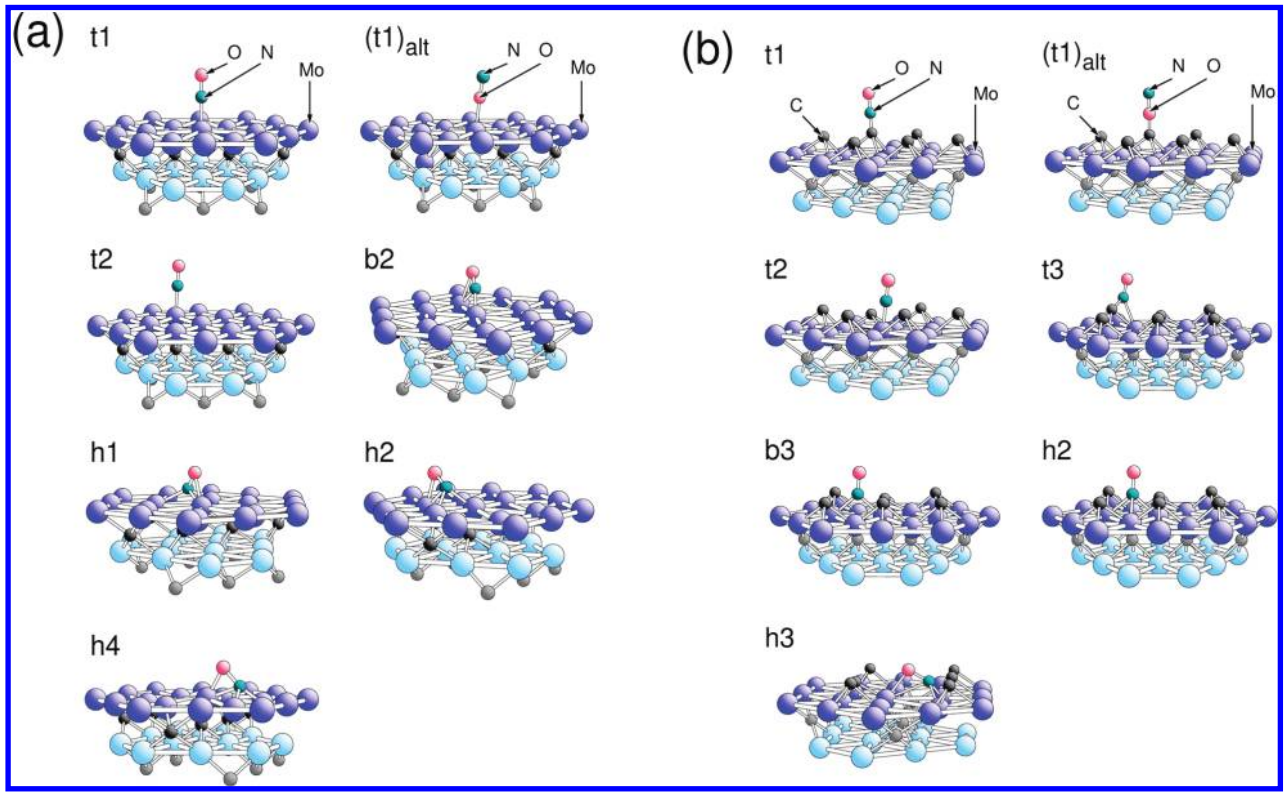

Figure 4. Equilibrium geometries of molecular NO adsorption at the β-$Mo_2C(0001)$ surface with (a) Mo termination and (b) C termination. Molybdenum (carbon, oxygen, nitrogen) atoms are shown by large (small) balls with different painting and connecting sticks visualizing atom coordination. The labels refer to adsorption sites as defined in Figure 2; see also text.

TABLE 2: Molecular NO Adsorption at β-$Mo_2C(0001)$ for (a) Mo Termination and (b) C Termination[a]

(a) Molybdenum Termination

site		E_{ads}	$d_{N-O}/d_{N-Mo}/d_{O-Mo}$	Q_{NO}
top	t1	−2.86	1.19/1.85/−	−0.40
	$(t1)_{alt}$	0.11	1.20/−/1.93	−0.41
	t2	−2.72	1.19/1.84/−	−0.40
bridge	b1	→ t1	−	−
	b2	−2.99	1.26/1.89, 2.20/2.26	−0.71
	b3	→ b2	−	−
	b4	→ h4	−	−
hollow	h1	−3.45	1.37/2.08, 2.09, 2.11/2.04	−1.02
	h2	−2.88	1.33/2.08, 2.09, 2.15/2.10	−0.82
	h3	→ h2	−	−
	h4	−2.70	1.42/2 × 2.11, 2.18/2.00	−1.05
free NO		−	1.18/−/ −	0.00

(b) Carbon Termination

site		E_{ads}	$d_{N-O}/d_{N-Mo}/d_{O-Mo}$	Q_{NO}
top	t1	−2.28	1.20/1.22/−	0.00
	$(t1)_{alt}$	0.86	1.22/−/−	−0.03
	t2	−1.86	1.18/1.84/−	−0.30
	t3	−1.41	1.23/2.18/−	−0.17
bridge	b1	→ t1	−	−
	b2	→ t2	−	−
	b3	−1.49	1.21/2.11, 2.13/−	−0.46
	b4	→ h2	−	−
hollow	h1	→ t1	−	−
	h2	−1.39	1.22/2.16, 2.13, 2.43/−	−0.50
	h3	−1.85	1.34/2 × 2.17, 2 69/2.14	−0.51

[a] The tables list NO adsorption energies E_{ads} (in eV), selected bond distances, d_{N-O}, d_{N-Mo}, and d_{O-Mo} (in Å), and Mulliken charges Q_{NO} of the NO adsorbate (in au). The adsorption sites are denoted as shown in Figure 2. Stable ($E_{ads} < 0$) or metastable ($E_{ads} > 0$) adsorption sites are included numerically, while unstable sites are denoted by arrows pointing to the nearest stable site; see text.

The present adsorption geometries of NO at the carbide surface, allowing very different surface sites, top, bridge, and hollow, can be compared with NO adsorption at single crystal surfaces of metals, such as rhodium. There, calculations indicate that the most favorable sites for NO adsorption are bridge sites on (100), (110) surfaces and hollow sites at the (111) surface,

respectively.[44–46] The different behavior has to be attributed to different atom packing as well atom composition in the two types of substrates.

Of the 10 different adsorption sites at the C-terminated surface (see Figure 2b), 6 sites, t1, t2, t3, b3, h2, and h3, lead to stable molecular adsorption, with equibrium geometries shown in Figure 4b. Calculated adsorption energies E_{ads}, selected equilibrium distances, and adsorbate net charges (from Mulliken analyses) are given in Table 2b. Here, the energetically preferred site is the top site t1, where NO adsorbs on top of a surface carbon to form a tilted CNO species (see Figure 4b) with $E_{ads} = -2.28$ eV. The other stable but less favorable sites are t2, h3, b3, t3, and h2 with $E_{ads} = -1.86$, -1.85, -1.49, -1.41, and -1.39 eV, respectively. In contrast, NO approaching near the b1, b2, b4, and h1 sites of the surface leads to adsorption at the t1, t2, h2, and t1 sites, respectively. Analogous to the Mo termination, the t1 site of the C termination offers an alternative adsorbate geometry where NO binds with its O end pointing toward the substrate and forming a NOC species, labeled $(t1)_{alt}$ in Table 2b and Figure 4b, which is metastable, with $E_{ads} = 0.86$ eV. Similar results have been found for NO adsorption on the W(111) surface by Chen et al.[47] Overall, adsorption energies of NO at the C-terminated surface turn out to be smaller in absolute size compared with those for the Mo-terminated surface, suggesting weaker chemisorptive bonds.

3.3. Atomic C, N, and O Adsorption at β-Mo_2C(0001). As before, 10 different adsorption sites at the Mo-terminated surface are considered (see Figure 2a), where 4 sites yield stable atomic adsorption of C, N, and O each. Calculated adsorption energies E_{ads} according to eq 1 and selected equilibrium distances are listed in Table 3a. For adsorption of atomic carbon, the hollow site h1 is energetically the most favorable, with $E_{ads} = -7.43$ eV, while the h4, h2, and h3 sites yield smaller adsorption energies in absolute size; see Table 3a. In contrast, C approaching near the t1, t2, b1, b2, b3, and b4 sites of the surface leads to adsorption at the h1, h4, h1, h1, h2, and h4 sites, respectively. For atomic nitrogen, adsorption at the h1 site is also energetically preferred, with $E_{ads} = -7.59$ eV, while the h2, h4, and b3 sites are less favorable. Further, N approaching near the t1, t2, b1, b2, b4, and h3 sites leads to adsorption at the h4, h1, h1, h1, h4, and b3 sites, respectively. Similar results were found for N adsorption at the Rh(211) metal surface where the hollow site was found to be most favorable, and bringing atomic nitrogen to a hollow site resulted in adsorption at a bridge site.[46] For atomic oxygen, the h1 and h2 sites yield the largest adsorption energies, $E_{ads} = -6.76$ and -6.69 eV, while the t1 and h4 sites yield smaller adsorption energies in absolute size; see Table 3a. In contrast, O approaching near the t2, b1, b2, b3, b4, and h3 sites leads to adsorption at the h1, h1, h1, h2, h4, and h2 sites, respectively.

Of the 10 different adsorption sites at the C-terminated surface (see Figure 2b), 4 sites yield stable atomic adsorption of C, N, and O, with adsorption energies E_{ads} and selected equilibrium distances listed in Table 3b. For adsorption of atomic carbon, the top site t3 is energetically the most favorable, with $E_{ads} = -7.69$ eV, while the h3, t2, and h2 sites yield smaller adsorption energies in absolute size; see Table 3b. In contrast, C approaching near the t1, b1, b2, b3, b4, and h1 sites of the surface leads to adsorption at the h3, h3, t3, h2, h3 and t3 sites, respectively. For atomic nitrogen, adsorption at the hollow site h3 is energetically preferred, with $E_{ads} = -7.14$ eV, while the t2, t3, and h2 sites are less favorable. Further, N approaching near the t1, b1, b2, b3, b4, and h1 sites results in adsorption at the h3, h3, t2, h2, h2, and t2 sites, respectively. For atomic oxygen, the t1 and t2 sites yield the largest adsorption energies, $E_{ads} = -5.84$ and -5.69 eV, while the h3 and h2 sites yield smaller adsorption energies in absolute size; see Table 3b. In contrast, O approaching near the t3, b1, b2, b3, b4, and h1 sites leads to adsorption at the t1, t1, h2, h2, h2, and t2 sites, respectively.

The present data for atom adsorption show clearly that, overall, nitrogen and carbon bind with the Mo_2C substrate more strongly than oxygen, with adsorption energies that are larger in absolute size for C and N compared with that for O. Further, N and C atoms are found to adsorb preferentially at hollow sites of the substrate surface, blocking other atoms from penetrating into the bulk. This is consistent with observations by Miki et al. and Chen et al., who suggested for the W(111) surface that atomic oxygen diffusion into the bulk is blocked by preadsorbed atomic nitrogen.[47,48]

3.4. Dissociative Adsorption of CO at β-Mo_2C(0001). Here, we examine dissociative adsorption of CO with C and O atoms stabilizing at adjacent sites of the β-Mo_2C(0001) surface, where only sites which lead to stable atom adsorption of the separate C and O species are considered in the selection. Thus, based on the results of section 3.3, carbon will always be assumed to occupy hollow sites, while oxygen can stabilize in top and hollow sites at the Mo-terminated surface. This results in 16 site pairs C(x)/O(y), where pairs C(h1)/O(h1) and C(h4)/O(h4) are excluded, with 14 pairs remaining. Of these, 8 site pairs yield stable dissociative CO adsorption. Calculated adsorption energies E_{ads}' according to eq 2 and selected equilibrium distances are given in Table 4a. Obviously, dissociative CO adsorption happens only for hollow/hollow site pairs, where C(h1)/O(h4) is energetically the most favorable with $E_{ads}' = -2.94$ eV followed by the C(h4)/O(h2) pair with $E_{ads}' = -2.64$ eV while the other 6 site pairs yield smaller adsorption energies in absolute size; see Table 4a.

The dissociation path, CO(h1) → C(h1)/O(h4), connecting the energetically most stable geometries of molecular and dissociative CO adsorption at the Mo-terminated β-Mo_2C(0001) surface is examined in detail by NEB calculations.[43] Figure 5a shows that the dissociation process happens by oxygen moving over a Mo top site (characterizing the transition state) to the nearest hollow site h4 while the carbon species remains near the initial h1 site. The dissociation path yields a barrier energy of 0.89 eV (see Figure 5a), and the vibrational analysis at the transition state shows an imaginary frequency of -477 cm^{-1}.

The analogous procedure of selecting site pairs for the C-terminated β-Mo_2C(0001) surface allows 15 site pairs C(x)/O(y), of which 7 pairs result in stable dissociative CO adsorption with adsorption energies E_{ads}' and selected equilibrium distances given in Table 4b. For this termination, the calculations yield dissociative CO adsorption with a hollow/hollow site pair only for C(h2)/O(h2), where the resulting geometry is metastable with $E_{ads}' = 0.69$ eV. On the other hand, the top/hollow site pair C(t3)/O(h3) is energetically preferred with $E_{ads}' = -2.29$ eV, followed by the hollow/top pair C(h3)/O(t1) with $E_{ads}' = -2.20$ eV. The latter includes oxygen in a top site above carbon, which suggests that dissociative CO adsorption at the C-terminated surface can also result in separate surface CO species, where oxygen moves from the adsorbate to a substrate carbon atom. The other six site pairs yield smaller adsorption energies in absolute size; see Table 4b. Further, the data of Table 4b suggest that dissociative adsorption at the C-terminated surface is, on average, energetically less favorable than that at the Mo-terminated surface.

The CO dissociation path at the C-terminated β-Mo_2C(0001) surface is somewhat more complicated compared with that at

TABLE 3: Atomic C, N, and O Adsorption at β-Mo_2C(0001) for (a) Mo Termination and (b) C Termination[a]

(a) Molybdenum Termination

site		E_{ads}(C)	d_{C-Mo}	E_{ads}(N)	d_{N-Mo}
top	t1	→ h1	−	→ h4	−
	t2	→ h4	−	→ h1	−
bridge	b1	→ h1	−	→ h1	−
	b2	→ h1	−	→ h1	−
	b3	→ h2	−	−5.90	1.92, 2.05
	b4	→ h4	−	→ h4	−
hollow	h1	−7.43	1.95, 2 × 2.04	−7.59	1.93, 2.03, 2.04
	h2	−6.80	2 × 2.00, 2.06	−7.14	1.99, 2.02, 1.98
	h3	−6.27	2.04, 2.19, 2.13	→ b3	−
	h4	−7.09	2 × 2.15, 2.17	−6.82	2.00, 2 × 2.03

site		E_{ads}(O)	d_{O-Mo}
top	t1	−6.08	1.74
	t2	→ h1	−
bridge	b1	→ h1	−
	b2	→ h1	−
	b3	→ h2	−
	b4	→ h4	−
hollow	h1	−6.76	2 × 2.06, 2.00
	h2	−6.69	2.03, 2.04, 2.10
	h3	→ h2	−
	h4	−6.17	2.09, 2.11, 2.10

(b) Carbon Termination

site		E_{ads}(C)	d_{C-Mo}/d_{C-C}	E_{ads}(N)	d_{N-Mo}/d_{N-C}
top	t1	→ h3	−	→ h3	−
	t2	−6.14	2.07/1.33	−6.76	2.22/1.24
	t3	−7.69	2.15/1.37,1.38	−6.17	2.18/2 × 1.35
bridge	b1	→ h3	−	→ h3	−
	b2	→ t3	−	→ t2	−
	b3	→ h2	−	→ h2	−
	b4	→ h3	−	→ h2	−
hollow	h1	→ t3	−	→ t2	−
	h2	−5.08	2.04, 2.08, 2.06/−	−5.32	2.06, 2.12, 1.99/−
	h3	−7.23	2.11, 2 ×2.23/1.36	−7.14	2 × 2.28, 2.24/1.28

site		E_{ads}(O)	d_{O-Mo}/d_{O-C}
top	t1	−5.84	−/1.19
	t2	−5.69	2.26/1.23
	t3	→ t1	−
bridge	b1	→ t1	−
	b2	→ h2	−
	b3	→ h2	−
	b4	→ h2	−
hollow	h1	→ t2	−
	h2	−5.04	2.06, 2.08, 2.21/−
	h3	−5.14	2 × 2.43, 2.91/1.25

[a] The tables list corresponding adsorption energies E_{ads} (in eV) and selected bond distances, d_{C-Mo}, d_{N-Mo}, and d_{O-Mo} (in Å). Further, distances d_{C-C}, d_{N-C}, and d_{O-C} are given for the C termination. The adsorption sites are denoted as shown in Figure 2. Stable ($E_{ads} < 0$) or metastable ($E_{ads} > 0$) adsorption sites are included numerically, while unstable sites are denoted by arrows pointing to the nearest stable site; see text.

the Mo-terminated surface. Here, NEB calculations suggest a two-step process for the energetically preferred path. In a first step, molecular CO diffuses from the terminal site t1 to the hollow site h3, yielding a barrier energy of 0.50 eV for the transition state TS1; see Figure 5b. Then, in a second step, molecular CO at the h3 site (CO_h in Figure 5b) dissociates by oxygen moving over a Mo top site (the transition state TS2) to a surface carbon t1 site, forming a surface CO species. This leads to a rather large barrier energy of 1.92 eV (see Figure 5b), and the vibrational analysis at the transition state shows an imaginary frequency of -548 cm^{-1}.

Altogether, the calculations show that dissociative CO adsorption for both terminations of the β-Mo_2C(0001) surface lead to quite stable structures. The range of adsorption energies (in eV), [−2.94, −1.51] and [−2.29, −0.23] for the Mo and C termination, respectively, is found to be shifted slightly to more negative E_{ads} values compared with the results for molecular adsorption yielding [−1.99, −1.11] and [−1.94, −0.78], respectively. This makes dissociative CO adsorption energetically somewhat more profitable compared with molecular adsorption, which may suggest that dissociative CO adsorption is more likely to happen. However, the difference between the two types is rather moderate. On the other hand, CO dissociation at the surface is accompanied by sizable barriers, which makes the process less likely to happen. This is confirmed by experimental results[16] which show that upon CO adsorption at

TABLE 4: Dissociative CO Adsorption at β-Mo_2C(0001) for (a) Mo Termination and (b) C Termination (see text)[a]

(a) Molybdenum Termination		
C/O site pairs	E_{ads}'	d_{C-Mo}/d_{O-Mo}
hollow/top		
C(h1)/O(t1)	−	−
C(h2)/O(t1)	−	−
C(h3)/O(t1)	−	−
C(h4)/O(t1)	−	−
hollow/hollow		
C(h1)/O(h2)	−1.64	1.94, 1.99, 2.08/1.95, 2.11, 2.19
C(h1)/O(h4)	−2.94	2.04, 2.04, 1.97/2.10, 2 × 2.11
C(h2)/O(h1)	−	−
C (h2)/O(h2)	−2.28	2.02, 2.03, 1.99/2.03, 2.06, 2.07
C(h2)/O(h4)	−2.21	1.97, 1.99, 2.12/3 × 2.10
C(h3)/O(h1)	−2.05	2.04, 2.19, 2.15/1.95, 2.09, 2.13
C(h3)/O(h2)	−1.51	2.06, 2.26, 2.28/2.01, 2.06, 2.10
C(h3)/O(h4)	−	−/−
C(h4)/O(h1)	−2.38	2 × 2.10, 1.94/2 × 2.07, 2.05
C(h4)/O(h2)	−2.64	2 × 2.11, 2.41/2.01, 2.12, 2.14
(b) Carbon Termination		
C/O site pairs	E_{ads}'	$d_{C-Mo}/d_{O-Mo}/d_{C-C}/d_{C-O}$
top/top		
C(t2)/O(t1)	−1.37	1.95/−/−/1.31, 1.46
C(t2)/O(t3)	−1.69	2.23/2.20/1.41, 1.33/1.30
C(t3)/O(t1)	−	−
C(t3)/O(t2)	−1.07	2.32/2.25, 2.30/1.37, 1.32/1.29
hollow/top		
C(h2)/O(t1)	−0.23	2.05, 2.08, 2.04/−/−/1.20
C(h2)/O(t2)	−	−
C(h3)/O(t1)	−2.20	2.16, 2 × 2.20/2.30/1.36/1.24
C(h3)/O(t2)	−	−
top/hollow		
C(t2)/O(h2)	−	−
C(t2)/O(h3)	−	−
C(t3)/O(h2)	−1.05	2.14/2.10, 2.17, 2.13/1.36, 1.39/−
C(t3)/O(h3)	−2.29	2.15/2.44, 2.41/1.37, 1.38/1.25
hollow/hollow		
C(h2)/O(h2)	0.69	1.99, 2.00, 2.07/2.02, 2.29, 2.05/−/−
C(h2)/O(h3)	−	−
C(h3)/O(h2)	−	−

[a] The table lists adsorption sites of corresponding C/O pairs, adsorption energies E_{ads}' (in eV) with molecular CO as a gas-phase reference, and selected bond distances, d_{C-Mo} and d_{O-Mo} (in Å). The adsorption sites are denoted as shown in Figure 2, where only sites of stable/metastable atom adsorption (see Table 3) are considered.

the Mo_2C substrate, at most, 10% of adsorbed CO undergoes decomposition.

3.5. Dissociative Adsorption of NO at β-Mo_2C(0001). Analogous to CO, dissociative adsorption of NO with N and O atoms stabilizing at adjacent sites of the β-Mo_2C(0001) surface is studied in calculations where only sites of stable N and O atom adsorption are included. This yields 14 site pairs N(x)/O(y) at the Mo-terminated surface with nitrogen in hollow and oxygen in both hollow and top sites. Of these, 11 site pairs are found to lead to stable dissociative NO adsorption. Calculated adsorption energies E_{ads}' according to eq 2 and selected equilibrium distances are given in Table 5a. Here, the N(h1)/O(h4) site pair is energetically the most favorable with $E_{ads}' = -5.89$ eV, followed by five site pairs with very similar adsorption energies E_{ads}' ranging between −5.57 and −5.37 eV, which are all hollow/hollow type; see Table 5a. The remaining five pairs of stable adsorption, which include the two hollow/top pairs, yield lower adsorption energies in absolute size. Similar results were found for dissociative NO adsorption at

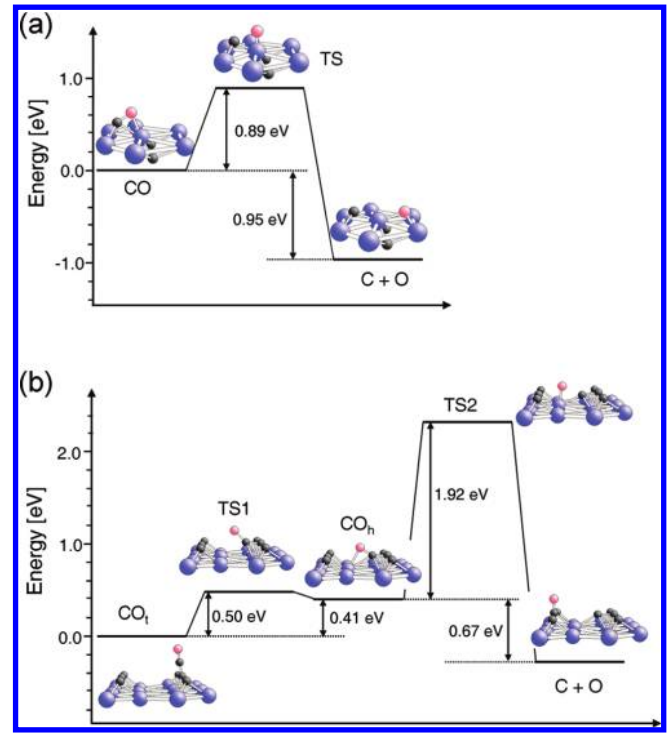

Figure 5. Reaction paths for CO dissociation at the (a) Mo-terminated and (b) C-terminated β-Mo_2C(0001) surfaces. The energy diagrams refer to equilibrium states of molecular (labeled CO) and dissociative adsorption (C + O) and include corresponding transition states (TS); see text. Labels CO_t and CO_h denote molecular CO adsorption near terminal and hollow sites, respectively, of the surface. Adsorbate geometries of initial and intermediate reaction steps are illustrated by ball-and-stick models of the local surface region.

the Rh(211) surface,[46] where the most favorable geometry is also described by N and O in adjacent hollow sites.

The NEB results for the most favorable dissociation path, NO(h1) → N(h1)/O(h4), at the Mo-terminated β-Mo_2C(0001) surface are shown in Figure 6a. Analogous to CO dissociation, the conversion of molecular NO to its atomic species occurs by oxygen moving over a Mo top site (the transition state) to the nearest hollow site h4 while the nitrogen species remains near the initial h1 site. This results in a barrier energy of only 0.26 eV (see Figure 6a), and the vibrational analysis at the transition state shows an imaginary frequency of −545 cm^{-1}. The barrier energy is consistent with data from earlier theoretical studies for low NO coverage at the Rh(100) surface yielding 0.50 eV.[49,50] Thus, the present calculations indicate that at the Mo-terminated β-Mo_2C(0001) surface, dissociation of NO (barrier energy of 0.26 eV) is much easier than dissociation of CO (barrier energy of 0.89 eV).

The aforementioned procedure of selecting site pairs for the C-terminated β-Mo_2C(0001) surface results in 15 pairs N(x)/O(y) with nitrogen and oxygen in both hollow and top sites, where 14 lead to stable dissociative NO adsorption with adsorption energies E_{ads}' and selected equilibrium distances given in Table 5b. For this termination, the N(h3)/O(t1) site pair is energetically the most favorable with $E_{ads}' = -5.33$ eV, while the other 13 site pairs yield smaller adsorption energies E_{ads}' in absolute size without a clear trend as to site preferences; see Table 5b. Interestingly, the energetically most favorable two site pairs, N(h3)/O(t1) and N(t3)/O(t1), include oxygen in top sites above carbon. Thus, analogous to CO discussed above, dissociative NO adsorption at the C-terminated surface will also result in formation of surface CO species. This is consistent

TABLE 5: Dissociative NO Adsorption at β-Mo_2C(0001) for (a) Mo Termination and (b) C Termination (see text)[a]

(a) Molybdenum Termination

N/O site pairs	E_{ads}'	d_{N-Mo}/d_{O-Mo}
hollow/top		
N(h1)/O(t1)	−	−
N(h2)/O(t1)	−4.80	2.15, 1.94, 1.91/1.74
N(h3)/O(t1)	−	−
N(h4)/O(t1)	−4.57	2.15, 2.12, 2.11/1.75
hollow/hollow		
N(h1)/O(h2)	−5.37	1.99, 2.05, 1.92/2.17, 1.96, 2.10
N(h1)/O(h4)	−5.89	1.94, 2 × 2.02/2.11, 2 × 2.08
N(h2)/O(h1)	−4.95	2.11, 1.92, 2.03/2.05, 2.13, 1.96
N(h2)/O(h2)	−5.51	2.04, 1.97, 1.98/2.07, 2.05, 2.04
N(h2)/O(h4)	−5.57	1.87, 2.37, 1.96/2.05, 2.09, 2.08
N(h3)/O(h1)	−4.57	1.98, 2.12, 2.13/2.00, 2.14, 2.07
N(h3)/O(h2)	−4.09	1.99, 2.09, 2.05/2.16, 2.17, 1.93
N(h3)/O(h4)	−	−
N(h4)/O(h1)	−5.49	1.98, 2.02, 2.01/2.04, 2 × 2.07
N(h4)/O(h2)	−5.46	1.97, 2.02, 2.06/2.10, 2.08, 2.01

(b) Carbon Termination

C/O site pairs	E_{ads}'	$d_{N-Mo}/d_{O-Mo}/d_{C-N}/d_{C-O}$
top/top	−	−
N(t2)/O(t1)		
N(t2)/O(t3)	−3.42	2.03/2.28/1.29/1.26
N(t3)/O(t1)	−5.08	2.26, 2.12/−/1.31/1.19
N(t3)/O(t2)	−4.01	2.33/2.26/1.37, 1.36/1.25
hollow/top		
N(h2)/O(t1)	−3.20	2.15, 2.07, 1.96/−/−/1.19
N(h2)/O(t2)	−2.88	2.11, 2.07, 1.97/2.35/−/1.22
N(h3)/O(t1)	−5.33	2 × 2.29/−/1.26/1.19
N(h3)/O(t2)	−4.93	2.26, 2.27/2.27/1.28/1.23
top/hollow		
N(t2)/O(h2)	−3.69	2.26, 2.48/2 × 2.19, 2.00/1.24/−
N(t2)/O(h3)	−4.37	2.22/2 × 2.42/1.24/1.25
N(t3)/O(h2)	−3.14	2.14/2.06, 2.21, 2.14/1.36, 1.39/−
N(t3)/O(h3)	−4.08	2.25/2.44, 2.42/1.34, 1.39/1.25
hollow/hollow		
N(h2)/O(h2)	−2.24	2.07, 2.11, 1.98/2.09, 2.06, 2.22/−/−
N(h2)/O(h3)	−3.19	−/2.00, 2.27, 1.99/−/1.21
N(h3)/O(h2)	−3.54	2.32, 2.14, 2.21/1.97, 2.36, 2.10/1.28/−

[a] The table lists adsorption sites of corresponding N/O pairs, adsorption energies E_{ads}' (in eV) with molecular NO as a gas-phase reference, and selected bond distances, d_{N-Mo} and d_{O-Mo} (in Å). The adsorption sites are denoted as shown in Figure 2, where only sites of stable/metastable atom adsorption (see Table 3) are considered.

with experimental findings from temperature-programmed desorption (TPD) studies for NO adsorbed at a β-Mo_2C substrate, where also desorption of CO was observed.[26]

As for CO dissociation, the preferred NO dissociation path at the C-terminated β-Mo_2C(0001) surface can be described as a two-step process, where, in a first step, molecular NO diffuses from the terminal site t1 to the hollow site h3. Here, the NEB calculations yield a barrier energy of 0.54 eV for the transition state TS1; see Figure 6b. In the second step, molecular NO at the h3 site (NO_h in Figure 6b) dissociates by oxygen moving over a Mo top site (the transition state TS2) to a surface carbon t1 site, forming a surface CO species. This leads to a moderate barrier energy of 0.72 eV (see Figure 6b), and the vibrational analysis at the transition state shows an imaginary frequency of -571 cm^{-1}. NO dissociation preceded by initial diffusion has also been reported for NO adsorbing at Pd[50] and Rh[46,50,51] metal surfaces.

Overall, the calculations show that dissociative NO adsorption for both terminations of the β-Mo_2C(0001) surface leads also to very stable geometries. The range of adsorption energies (in eV), [−5.89, −4.09] and [−5.33, −2.24] for the Mo and C termination, respectively, turns out to be shifted considerably to more negative E_{ads} values compared with the results for molecular adsorption, [−3.45, −2.70] and [−2.28, −1.39], respectively. Thus, dissociative NO adsorption is energetically much more profitable than molecular adsorption, which indicates strongly that NO will dissociate at the β-Mo_2C(0001) surface. This is consistent with earlier theoretical results for the Mo-terminated α-Mo_2C surface, where dissociative adsorption was found to be preferable over molecular adsorption.[31] It also confirms experiments which show that upon NO adsorption at the Mo_2C substrate, almost all NO molecules dissociate.[16]

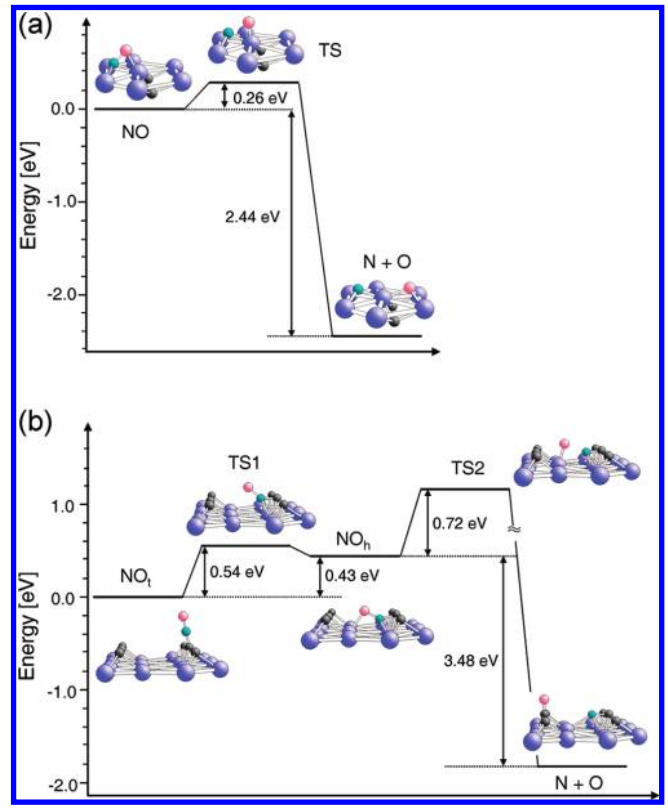

Figure 6. Reaction paths for NO dissociation at the (a) Mo-terminated and (b) C-terminated β-Mo_2C(0001) surfaces. The energy diagrams refer to equilibrium states of molecular (labeled NO) and dissociative adsorption (N + O) and include corresponding transition states (TS); see text. Labels NO_t and NO_h denote molecular NO adsorption near terminal and hollow sites, respectively, of the surface. Adsorbate geometries of initial and intermediate reaction steps are illustrated by ball-and-stick models of the local surface region.

3.6. Vibrational Analysis of the Adsorbates. Characteristic vibrational frequencies ν for molecular CO and NO adsorbates as well as adsorbed O and N atoms on the Mo- and C-terminated β-Mo_2C(0001) surface are listed in Table 6. Here, calculated ν values of the molecular adsorbates are restricted to a range between 900 and 4000 cm^{-1}, which reflects the experimental range considered in the IR measurement for adsorption at a β-Mo_2C catalyst.[17,18,22] For atomic O and N adsorption, the theoretical frequencies are confined between 400 and 1800 cm^{-1}, while corresponding experimental IR data range between 800 and 1300 cm^{-1}.[16,17] Further, the comparison between theory and experiment in Table 6 includes assignments to adsorption sites and surface termination and combines computed vibrational frequencies for adsorption at different surface terminations in a given frequency range. As a main result, the theoretical results confirm most of the experimental assignments but also yield additional information.

TABLE 6: Vibrational Frequencies ν (in cm^{-1}) of CO and NO, N, and O Adsorbed at the β-Mo_2C(0001) Surface for Mo and C Termination, Labeled T_{Mo} and T_C, Respectively[a]

	experiment		theory	
adsorbate	ν	site	ν	site
CO	2364[b]	CO_2[b]	–	–
	2196[c], 2179[b]	top C[c]	2213	t1(T_C)
	2112[b]	–	2071	t2(T_C)
	2057[d], 2054[c]	top ads[d], top Mo[c]	2071	t2(T_C)
	1626[b]	–	1616, 1633	h3(T_C), b2(T_{Mo})
	–	–	1806	t1(T_{Mo})
	1450[b]	CO polymer[b]	1397	h1(T_{Mo})
NO	1780[d]	top ads[d]	1809, 1809, 1789	t2(T_{Mo}, T_C), t1(T_{Mo})
	–	–	1716	t3(T_C)
	–	–	2156, 1322	t1(T_C)
			1193	t3(T_C)
O	989, 942[e]	top Mo[e]	898	t1(T_{Mo})
	–	–	360, 474, 545, 1589	t2(T_C)
N	–	–	1763, 527, 460	t2(T_C)
	–	–	1241, 1046	t3(T_C)
	–	–	559, 545, 517	t3(T_C)
	–	–	470, 615, 622	h1(T_{Mo})

[a] The table compares experimental data with theoretical results and includes assignments to adsorption sites and surface termination. [b] Reference 22. [c] Reference 18. [d] Reference 16. [e] Reference 17.

For CO adsorption, two main peaks at about 2200 and 2050 cm^{-1} are observed in the experiment.[16,18,22] The former is assigned to the CO adsorption in top sites above C substrate atoms, while the latter is claimed to be due to adsorption on top of Mo substrate atoms.[16,18] This is consistent with the calculated stretching frequencies of CO adsorbed on top of C and Mo sites of the C-terminated surface, yielding 2213 and 2071 cm^{-1}, respectively; see Table 6. In contrast, calculated vibrations for CO on top of Mo sites of the Mo-terminated surface result in a frequency of 1806 cm^{-1}, where the experimental spectra do not show a clear peak structure. An additional peak in the experimental spectra at 2364 cm^{-1} has been attributed to CO_2 vibrations,[22] which cannot be confirmed by the present calculations. Further, there are peaks in experiment at 1626 and 1450 cm^{-1} which have been assigned to stretching vibrations of CO near Mo surface sites and to negatively charged CO polymers, respectively.[22] From the calculations, the former frequency may be associated with CO in either hollow sites at the C-terminated surface or at bridge sites of the Mo termination. The latter frequency can be explained by theory as due to vibrations of CO adsorbed in hollow site of the Mo termination.

For NO adsorption on a clean β-Mo_2C film, RAIRS experiments show a coverage-dependent shifting from 1780 cm^{-1} at low coverage to 1820 cm^{-1} at saturation coverage at 100 K.[16] This peak was attributed to a terminally bound NO species at top sites of the surface. This is consistent with computed frequencies for NO top adsorption above Mo substrate atoms of the Mo- and C-terminated surface; see Table 6. The calculations yield additional frequencies at 2124, 1322, and 1193 cm^{-1}, referring to top-site-adsorbed species, where the first two originate from vibrations of surface CNO species; see Figure 4b (t1 adsorption). These theoretical frequencies have not been observed in experiment.[16,17] Further, the calculations identify vibrations of NO adsorbed in bridge and hollow sites at the β-Mo_2C(0001) surface with frequencies between 914 and 1624 cm^{-1}, which have not been experimentally verified either.

Siaj et al. studied the dissociative adsorption of NO at the β-Mo_2C substrate by RAIRS and found a peak at 989 cm^{-1} with a shoulder at 942 cm^{-1}; see Table 6.[17] The two frequencies were attributed to vibrational modes of oxygen in top sites above Mo substrate atoms, reflecting O−Mo stretching, while N−Mo stretching vibrations were excluded in the interpretation. This is confirmed by the present calculations where O−Mo stretching vibrations of oxygen adsorbed in top sites of the Mo-terminated surface yield a frequency of 898 cm^{-1} while hollow site adsorption of oxygen results in vibrational frequencies between 343 and 570 cm^{-1}. Further, the calculations show a frequency of 1589 cm^{-1} for oxygen adsorbed near Mo sites of the C-terminated surface, which is due to C−O stretching vibrations, suggesting that oxygen, even when adsorbed near Mo surface sites, can form local CO surface groups. According to the calculations, atomic nitrogen stabilizes on top of Mo substrate atoms at the C- (but not at the Mo-) terminated surface. Computed frequencies of corresponding N−Mo stretching vibrations range between 460 and 559 cm^{-1}, and similar values are found for bridge and hollow sites of nitrogen at the C- and Mo-terminated surfaces. Thus, they cannot explain the peak at 989 cm^{-1} observed in the RAIRS experiment.[17] This applies also to higher-lying frequencies at 1046 and 1241 cm^{-1} obtained in the calculations for the C termination, which are characterized by complex modes of local groups involving N, Mo, and C atoms at the surface. Finally, the largest theoretical frequency of 1763 cm^{-1} found for the C-terminated surface reflects N−C stretching vibrations due to the formation of local surface CN groups.

3.7. Adsorption-Induced Activation of C−O and N−O Bonds. Adsorption of CO and NO at the differently terminated β-Mo_2C(0001) surface is accompanied by charge transfer between the adsorbate and the substrate, resulting, for almost all surface sites, in a negatively charged adsorbate species. This is evident from the Mulliken charges listed in Tables 1 and 2, which give a qualitative account of charging. The negative charging is connected with partial occupation of antibonding orbitals of the CO and NO adsorbates which weakens their interatomic bonds and leads to increased interatomic distances d_{C-O} and d_{N-O}; see Tables 1 and 2. This is connected with activation at the catalyst surface and can be considered as a first step toward dissociation of the adsorbates. As an illustration, Figure 7 shows the distances d_{C-O} and d_{N-O} of the two adsorbates at different sites of the Mo-terminated β-Mo_2C(0001) surface as a function of the amount of charge transferred, where

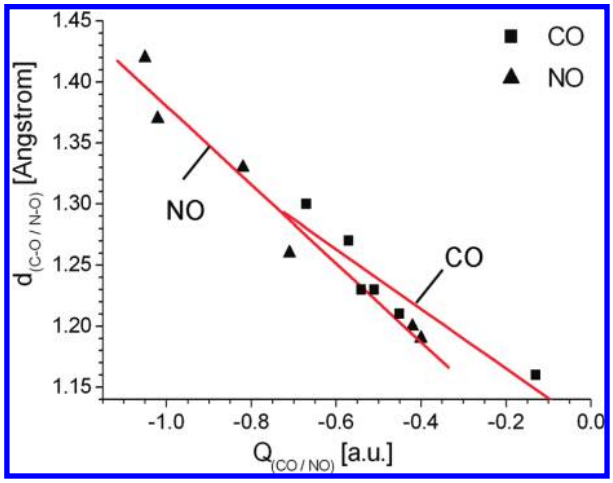

Figure 7. Interatomic distances d_{C-O} and d_{N-O} of CO and NO adsorbates at different sites of the Mo-terminated β-Mo_2C(0001) surface as a function of the charge transferred from substrate to adsorbate. The numerical results are taken from Mulliken charges Q_{CO} and Q_{NO}, respectively; see text. Data for CO are indicated by squares, and those for NO are denoted by triangles. The straight lines refer to least-squares fits.

the numerical results are taken from Mulliken charges Q_{CO} and Q_{NO}, respectively, listed in Tables 1 and 2. Obviously, for both adsorbate molecules, the interatomic distances increase linearly with increasing negative charge, where the slope $\Delta d/\Delta Q$ is given by -0.25 (Å/e) for CO and by -0.32 (Å/e) for NO, with e denoting an electron charge unit. For comparison, the $\Delta d/\Delta Q$ value for gas-phase CO in going from neutral CO to CO^- is calculated as -0.10 (Å/e) and that for NO in going from neutral NO to NO^- as -0.12 (Å/e). The linear relationship between interatomic distance and transferred charge has been also verified for CO adsorption at the Fe_4C surface as well as for CO_2 chemisorption on the transition-metal surfaces and seems to be of more general importance.[52,53] Thus, the degree of activation of the adsorbate, represented by its increase in interatomic distance, seems to be linearly related to the amount of negative charge transferred from the substrate to the adsorbate, and the degree of activation of C−O and N−O bonds may be increased by improving the surface ability to transfer electrons to the adsorbate.

At the C-terminated β-Mo_2C(0001) surface, the amount of adsorbate charging is overall much smaller for corresponding sites compared with that for the Mo-terminated surface; see Tables 1b and 2b. Further, there is no clear dependence of the interatomic distances d_{C-O} and d_{N-O} of the two adsorbates on the amount of charge transfer. This is explained by the fact the C-terminated surface is rather inhomogeneous as a result of the open arrangement of substrate carbon at the surface which is more mobile than molybdenum. This leads to very different complex local binding geometries involving CCO, CNO, MoCO, and MoNO groups such that substrate−adsorbate charge transfer is not as well-defined as for the flat Mo-terminated surface.

4. Conclusions

The present theoretical cluster studies provide detailed information on the molecular and dissociative adsorption of CO and NO at the Mo- as well as C-terminated β-Mo_2C(0001) surface. The studies, applying large surface clusters together with DFT methods to evaluate electronic, structural, and energetic parameters, show that at the Mo-terminated surface, both molecular CO and NO can adsorb in top, bridge, and hollow sites. Adsorption energies are found to be rather similar for stable sites and the same adsorbate, with NO binding more strongly to the surfaces than CO. At the C-terminated surface, the calculated adsorption energies are overall smaller in absolute size, suggesting weaker chemisorptive binding where CO can stabilize only in top and hollow but not in bridge sites. The weaker binding is clearly due to the carbon substrate atoms at the surface getting involved in the adsorbate bond, forming more complex local adsorbate groups.

Atomic C, N, and O adsorption at both terminations of the Mo_2C(0001) surface yields quite large adsorption energies in absolute size. This suggests very strong chemisorption, where at the Mo-terminated surface, hollow sites are energetically preferred. For the C termination, only oxygen is found to adsorb near carbon sites, forming a surface CO species, whereas C and N stabilize above Mo substrate atoms or in hollow sites. Overall, nitrogen and carbon bind with the Mo_2C substrate more strongly than oxygen, with adsorption energies that are larger in absolute size for C and N compared with that for O.

Further, the calculations show that dissociative CO adsorption for both terminations of the β-Mo_2C(0001) surface leads to quite stable geometries, where adsorption at the C-terminated surface is, on average, energetically less favorable than that at the Mo-terminated surface. Dissociative CO adsorption is found to be energetically somewhat more profitable compared with molecular adsorption where, however, the difference is rather moderate. Further, calculations for the reaction path connecting the energetically most stable geometries of molecular and dissociative adsorption at the Mo-terminated surface yield a reasonably high barrier energy of 0.89 eV, which can explain experimental results showing that upon CO adsorption at Mo_2C substrate, at most 10% of adsorbed CO undergoes decomposition.[16] Dissociative NO adsorption for both terminations of the β-Mo_2C(0001) surface results also in very stable geometries, where the Mo-terminated surface is energetically favored. Here, adsorption energies for dissociative adsorption are about twice as large in absolute size compared with those for molecular adsorption. This makes dissociative adsorption energetically much more profitable than molecular adsorption and indicates strongly that NO will dissociate at the β-Mo_2C(0001) surface. These findings are supported by calculations of optimized reaction paths for the Mo-terminated surface which yield a quite small barrier energy of 0.26 eV. They are also consistent with experimental results that indicate that upon NO adsorption at the Mo_2C substrate, almost all NO molecules dissociate.[16] Barrier energies of molecular CO and NO dissociation are found to be much higher for the C-terminated than those for the Mo-terminated surface such that dissociation is much less likely to happen at the C-terminated surface.

Computed vibrational modes and frequencies of adsorbed CO and NO allow a detailed interpretation and assignment of the different features in the experimental spectra obtained by IR spectroscopy, which confirms most of the experimental assignments but also yields additional information as to possible vibrational modes not observed or unexplained so far. In particular, the theoretical frequency analysis gives clear evidence that the peak at 989 cm^{-1} observed in experiments upon dissociative NO adsorption at the Mo_2C substrate results from oxygen vibrating on top of Mo substrate atoms.

Acknowledgment. This work was partly supported by the Deutsche Forschungsgemeinschaft (DFG) through its Collaborative Research Center Sfb 546, Transition metal oxide aggregates, and by the National Natural Science Foundation of China, Nos.

20590363, 20876163, and 10979068, by the State Key Fundamental Research Program, No. 2007CB216401. One of the authors (X.S.) is grateful for a stipend from the Max-Planck Society, allowing for performance of this work while visiting the Fritz-Haber-Institut Berlin (Germany).

References and Notes

(1) Liao, J. J.; Wilcox, R. C.; Zee, R. H. *Scr. Metall. Mater.* **1990**, *24*, 1647.
(2) Hwu, H. H.; Chen, J. G. *Chem. Rev.* **2005**, *105*, 185.
(3) Nelson, J. A.; Wagner, M. J. *Chem. Mater.* **2002**, *14*, 4460.
(4) Lee, J. S.; Yeom, M. H.; Lee, D.-S. *J. Mol. Catal.* **1990**, *62*, 145.
(5) Lee, J. S.; Yeom, M. H.; Park, K. Y.; Nam, I.-S.; Chung, J. S.; Kim, Y. G.; Moon, S. H. *J. Catal.* **1991**, *128*, 126.
(6) Lee, J. S.; Locatelli, S.; Oyama, S. T.; Boudart, M. *J. Catal.* **1990**, *125*, 157.
(7) Ledoux, M. J.; Pham-Huu, C.; Dunlop, H. M.; Guille, J. *J. Catal.* **1992**, *134*, 383.
(8) Aegerter, P. A.; Quigley, W. W. C.; Simpson, G. J.; Ziegler, D. D.; Logan, J. W.; McCrea, K. R.; Glazier, S.; Bussell, M. E. *J. Catal.* **1996**, *164*, 109.
(9) Yang, S.; Li, C.; Xu, J.; Xin, Q. *Chem. Commun.* **1997**, *13*, 1247.
(10) Yang, S.; Li, C.; Xu, J.; Xin, Q. *J. Phys. Chem.* **1998**, *36*, 6986.
(11) Peri, J. B. *J. Phys. Chem.* **1982**, *86*, 1615.
(12) Zaki, M. I.; Vielhaber, B.; Knözinger, H. *J. Phys. Chem.* **1986**, *90*, 3176.
(13) Lee, J. S.; Lee, K. H.; Lee, J. Y. *J. Phys. Chem.* **1992**, *96*, 362.
(14) Müller, B.; Van Langeveld, A. D.; Moulijn, J. A.; Knözinger, H. *J. Phys. Chem.* **1993**, *97*, 9028.
(15) Diaz, A. L.; Bussell, M. E. *J. Phys. Chem.* **1993**, *97*, 470.
(16) Wang, J.; Castonguay, M.; Deng, J.; McBreen, P. H. *Surf. Sci.* **1997**, *374*, 197.
(17) Siaj, M.; Maltais, C.; Zahidi, E. M.; Oudghiri-Hassani, H.; Wang, J.; Rosei, F.; Mcbreen, P. H. *J. Phys. Chem. B* **2005**, *109*, 15376.
(18) Wu, W.; Wu, Z.; Liang, C.; Chen, X.; Ying, P.; Li, C. *J. Phys. Chem. B* **2003**, *107*, 7088.
(19) Dubois, J.; Epicier, T.; Esnouf, C.; Fantozzi, G.; Convert, P. *Acta Metall.* **1988**, *8*, 1891.
(20) Epicier, T.; Dubois, J.; Esnouf, C.; Fantozzi, G.; Convert, P. *Acta Metall.* **1988**, *8*, 1903.
(21) Shi, X.-R.; Wang, S.-G.; Wang, H.; Deng, C.-M.; Qin, Z.; Wang, J. *Surf. Sci.* **2009**, *603*, 851.
(22) Tominaga, H.; Nagai, M. *J. Phys. Chem. B* **2005**, *109*, 20415.
(23) Tominaga, H.; Nagai, M. *Appl. Catal., A* **2007**, *328*, 35.
(24) Tominaga, H.; Nagai, M. *Appl. Catal., A* **2008**, *343*, 95.
(25) Haines, J.; Léger, J. M.; Chateau, C.; Lowther, J. E. *J. Phys.: Condens. Matter* **2001**, *13*, 2447.
(26) Pistonesi, C.; Juan, A.; Farkas, A. P.; Solymosi, F. *Surf. Sci.* **2008**, *602*, 2206.
(27) Parthé, E.; Sadagopan, V. *Acta Crystallogr.* **1963**, *16*, 202.
(28) Hammer, B.; Hansen, L. B.; Nørskov, J. K. *Phys. Rev. B* **1999**, *59*, 7413.
(29) Ren, J.; Huo, C.-F.; Wang, J.; Li, Y.-L.; Jiao, H. *Surf. Sci.* **2005**, *596*, 212.
(30) Ren, J.; Huo, C.-F.; Wang, J.; Cao, Z.; Li, Y.-L.; Jiao, H. *Surf. Sci.* **2006**, *600*, 2329.
(31) Ren, J.; Wang, J.; Huo, C.-F.; Wen, X.-D.; Cao, Z.; Yuan, S.; Li, Y.; Jiao, H. *Surf. Sci.* **2007**, *601*, 1599.
(32) Liu, P.; Rodriguez, J. A.; Hou, H.; Muckerman, J. T. *J. Chem. Phys.* **2003**, *118*, 7737.
(33) Liu, P.; Rodriguez, J. A. *Catal. Lett.* **2003**, *91*, 247.
(34) Liu, P.; Rodriguez, J. *J. Chem. Phys.* **2004**, *120*, 5414.
(35) Liu, P.; Rodriguez, J.; Asakura, T.; Gomes, J.; Nakamura, K. *J. Phys. Chem. B* **2005**, *109*, 4575.
(36) Liu, P.; Rodriguez, J. A. *J. Phys.Chem. B* **2006**, *110*, 19418.
(37) Viñes, F.; Sousa, C.; Illas, F.; Liu, P.; Rodriguez, J. A. *J. Phys.Chem. C* **2007**, *111*, 16982.
(38) Liu, P.; Lightstone, J. M.; Patterson, M. J.; Rodriguez, J. A.; Muckerman, J. T.; White, M. G. *J. Phys.Chem. B* **2006**, *110*, 7449.
(39) Lightstone, J. M.; Patterson, M. J.; Liu, P.; White, M. G. *J. Phys.Chem. A* **2006**, *110*, 3505.
(40) Kitchin, J. R.; Nørskov, J. K.; Barteau, M. A.; Chen, J. G. *Catal. Today* **2005**, *105*, 66.
(41) Perdew, J. P.; Burke, K.; Ernzerhof, M. *Phys. Rev. Lett.* **1996**, *77*, 3865.
(42) Hermann, K.; Pettersson, L. G. M.; Casida, M. E.; Daul, C.; Goursot, A.; Koester, A.; Proynov, E.; St-Amant, A.; Salahub, D. R.; Carravetta, V.; Duarte, H.; Friedrich, C.; Godbout, N.; Guan, J.; Jamorski, C.; Leboeuf, M.; Leetmaa, M.; Nyberg, M.; Pedocchi, L.; Sim, F.; Triguero, L.; Vela, A. *StoBe Software*; 2008.
(43) Jónsson, H.; Mills, G.; Jacobsen, K. W. Nudged Elastic Band Method for Finding Minimum Energy Paths of Transitions. In *Classical and Quantum Dynamics in Condensed Phase Simulations*; Berne, B. J., Ciccotti, G., Coker, D. F., Eds.; World Scientific: River Edge, NJ, 1998; p 385.
(44) Popa, C.; van Bavel, A. P.; van Santen, R. A.; Flipse, C. F. J.; Jansen, A. P. J. *Surf. Sci.* **2008**, *602*, 2189.
(45) Jia, X. F.; Yu, S. Q.; Wang, Z. X.; Ma, Y. S. *Surf. Interface Anal.* **2008**, *40*, 1350.
(46) Rempel, J.; Greeley, J.; Hansen, L. B.; Nielsen, O. H.; Nørskov, J. K.; Mavrikakis, M. *J. Phys. Chem. C* **2009**, *113*, 20623.
(47) Chen, H.-T.; Chen, H.-L.; Ju, S.-P.; Musaev, D. G.; Lin, M. C. *J. Phys. Chem. C* **2009**, *113*, 5300.
(48) Miki, H.; Irokawa, K.; Nitta, M.; Takeuchi, K.; Kioka, T. *Surf. Sci.* **1999**, *433*, 272.
(49) Loffreda, D.; Delbecq, F.; Simon, D.; Sautet, P. *J. Chem. Phys.* **2001**, *115*, 8101.
(50) Loffreda, D.; Simon, D.; Sautet, P. *J. Catal.* **2003**, *213*, 211.
(51) Tian, K.; Tu, X.-Y.; Dai, S.-S. *Surf. Sci.* **2007**, *601*, 3186.
(52) Wang, S.-G.; Liao, X.-Y.; Cao, D.-B.; Huo, C.-F.; Li, Y.; Wang, J.-W.; Jiao, H. *J. Phys. Chem. C* **2007**, *111*, 16934.
(53) Deng, C.-M.; Huo, C.-F.; Bao, L.-L.; Feng, G.; Li, Y.-W.; Wang, J.; Jiao, H. *J. Phys. Chem. C* **2008**, *112*, 19018.

JP912036Z